First contact in a viscous fluid

Chris Cawthorn

January 12, 2009

1 Introduction

Lubrication theory has been successfully applied to many problems in fluid dynamics. For cases where two objects slide past each other, with a thin film of fluid filling the intervening gap, it performs admirably, and its application has formed the basis for many important advancements in engineering. Furthermore, it appears in most undergraduate courses in fluid mechanics (see [1], for example). However, when used to model the coming together of two solid objects separated by a viscous fluid, the predictions of lubrication theory are decidedly unphysical.

Consider the simple example of a rigid cylinder settling under gravity towards a rigid, horizontal plane, as illustrated by Figure 1. The thickness of the gap between the cylinder and the plane is denoted by $h(x)$, where x is a horizontal coordinate measured relative to an origin situated at the intersection of the horizontal plane and the axis of symmetry. Under the approximation key to lubrication theory (the so-called 'lubrication approximation', which is valid provided that $\epsilon \mathrm{Re} \ll 1$), we ignore horizontal variations relative to the much faster vertical variations when calculating the horizontal velocity, and assume that the pressure only varies in the horizontal coordinate x. We find that the horizontal velocity has a parabolic profile

$$u(x,z) = -\frac{1}{2\mu}\frac{\partial p}{\partial x} z[h(x) - z],$$

which gives rise to a horizontal volume flux

$$Q(x) = -\frac{h^3}{12\mu}\frac{\partial p}{\partial x}.$$

Balancing this against the volume that must be squeezed out due to the settling of the cylinder, we find the so-called *Reynolds equation* for the pressure gradient

$$\frac{\partial}{\partial x}\left[-\frac{h^3}{12\mu}\frac{\partial p}{\partial x} + xR\dot{\epsilon}\right] = 0 \tag{1}$$

The dominant contribution to the upward resistive force on the cylinder comes from the pressure force

$$F_z = \int p \,\mathrm{d}x \propto \frac{\mu R\dot{\epsilon}}{\epsilon^{3/2}}.$$

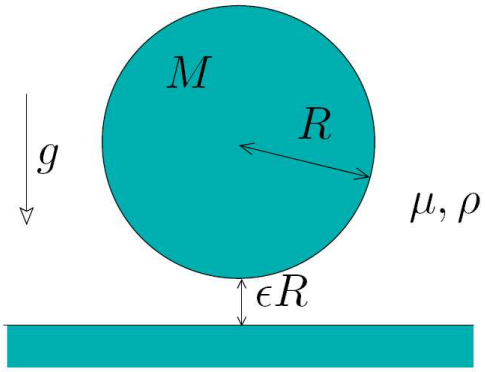

Figure 1: A simple application of lubrication theory. A rigid cylinder settles toward a rigid, horizontal plane under gravity.

The integration of the Reynolds equation (1) is straightforward, and can be well approximated analytically by extending the range of integration to $-\infty < x < \infty$, and approximating the gap thickness $h(x)$ by a parabola. The important result of this analysis is the scaling of the vertical force. Balancing this resistive force against the cylinder's weight (neglecting inertia, consistent with the lubrication approximation), we find that

$$Mg \propto \dot{\epsilon}\epsilon^{3/2} \tag{2}$$

$$\Rightarrow \epsilon(t) \propto (t - t_c)^{-2}. \tag{3}$$

So, according to lubrication theory, the cylinder (or indeed any object with a locally parabolic shape) takes an infinite length of time to make contact with the plate[1]. Such a result is clearly unphysical. It is the purpose of this report to address some possibilities for resolving this inconsistency.

Many physical effects could be introduced in order to attempt to capture finite-time contact. Perhaps small asperities on the solid surfaces will provide sharper, more streamlined points of contact between the two objects. Perhaps elasticity in the solid objects or compressibility in the fluid will provide a mechanism by which the large lubrication pressures can be mitigated. If these continuum scale effects are insufficient, then perhaps an explanation in terms of long range (e.g. Van der Waals) forces can be sought. In this report, we investigate the effects of roughness, elasticity and compressibility on settling problems, and see if contact in finite time can be achieved.

2 Roughness

Real surfaces are seldom perfectly smooth, as shown by Figure 2. When considering the effect of surface roughness on settling problems, we should first point out that the lubrication approximation itself is not the sole cause of the unphysical infinite contact time. A theorem of Gérard-Varet & Hillairet [2] states that, for a sufficiently smooth object settling toward

[1]For particularly flat shapes with zero local curvature, a similar analysis can be performed – see [5]

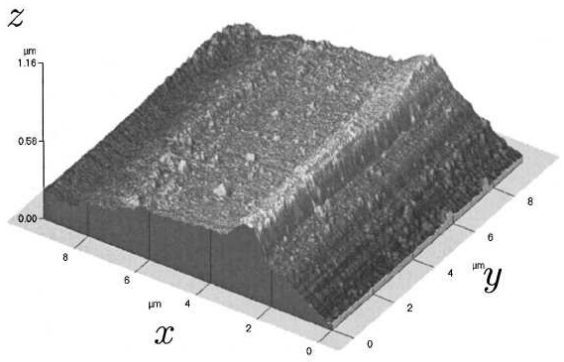

Figure 2: Atomic force micrograph of a roughness on a machined surface. Note rough asperities on the scale of microns. Picture copied from [3].

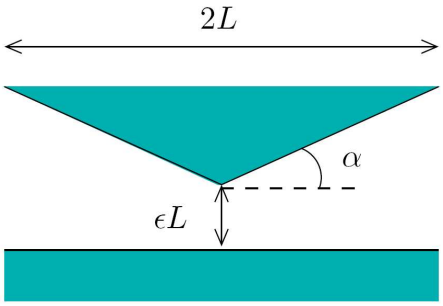

Figure 3: Diagram and notation for falling wedge

a sufficiently smooth plane under a constant body force, even the full, two-dimensional, Navier-Stokes equations require that contact will not occur in finite time. In order to resolve the problem without adding new physical processes (such as elasticity or compressibility, as discussed in §§3-4), we much insist that the settling objects contain sharp regions. By sharp, we mean regions where the first derivative of the surface function is discontinuous. In this section, we first consider the dynamics of a single sharp wedge settling in isolation, then move on to consider whether sharp roughness superimposed on a cylinder can change the settling dynamics as it rolls down an inclined plane.

2.1 Settling of a sharp wedge

In order to investigate the effect of a sharp asperity on contact, we consider the model problem of a falling wedge, as illustrated in Figure 3. The wedge is symmetric about $x = 0$, has width $2L$ and is pitched at angle α to the horizontal. We denote the closest approach of the wedge by ϵL. Assuming that the resulting flow has sufficiently small Reynolds number, we aim to solve the problem in a quasi-static manner, scaling out the settling velocity $\dot{\epsilon}$, and using the Stokes equations to find the resulting dimensionless hydrodynamical force F_Z as

a function of ϵ. We then use instantaneous force balance to equate the effective weight Mg' of the wedge with this hydrodynamic resistance. In this section, we detail two approximate analytic solutions for the Stokes velocity field, and present an exact numerical solution for comparison. Throughout this section, we shall nondimensionalise lengths with L, velocities with $\dot{\epsilon}L$, time with $\dot{\epsilon}^{-1}$, and pressure with $\mu\dot{\epsilon}$.

2.1.1 Lubrication solution

We begin by considering the flow obtained by applying the lubrication approximation to the flow beneath the falling wedge. The local thickness of the fluid layer is given by,

$$H(X) = \epsilon + |X| \tan\alpha. \tag{4}$$

Away from the sharp vertex at $X = 0$, we can expect the lubrication approximation to be reasonable provided that $\tan\alpha \ll 1$. For now, we shall not worry about the rapid horizontal variations in the vicinity of the vertex, except to note that the lubrication approximation should not be expected to perform well in this region.

After obtaining the Poisseuille velocity profile typical of lubrication flows

$$U(X,Z) = -\frac{1}{2}\frac{\partial P}{\partial X} Z\left[H(X) - Z\right], \tag{5}$$

we can integrate across the narrow gap to find the volume flux

$$Q(X) = \int_0^{H(X)} U(X,Z)\,\mathrm{d}X = -\frac{1}{12}\frac{\partial P}{\partial X} H^3$$

and use the local continuity relation to determine the Reynolds equation

$$\frac{\partial}{\partial X}\left[X - \frac{1}{12}\frac{\partial P}{\partial X} H^3\right] = 0. \tag{6}$$

By choosing the reference pressure so that we may take $P(X = \pm 1) = 0$, we can integrate equation (6) in order to determine the pressure gradient

$$\frac{\partial P}{\partial X} = \frac{12X}{H^3}. \tag{7}$$

We may now use (7) to calculate the upward resistive force

$$F_Z = \int_{-1}^{1} P\,\mathrm{d}X = -\int_{-1}^{1} X\frac{\partial P}{\partial X}\,\mathrm{d}X = -\frac{24}{\tan^3\alpha}\left[\log\epsilon - \frac{3}{2} + \mathcal{O}(\epsilon)\right], \tag{8}$$

and balance this against the weight of the wedge to determine the equation governing its vertical motion. Restoring dimensions, we have

$$\mu\dot{\epsilon}L\left[\log\epsilon - \frac{3}{2} + \mathcal{O}(\epsilon)\right] = -\frac{Mg'\tan^3\alpha}{24}. \tag{9}$$

Integrating (9), we find that the minimum separation ϵ is governed by

$$\epsilon\log\epsilon \sim \frac{Mg'\tan^3\alpha}{24\mu L}(t_1 - t), \tag{10}$$

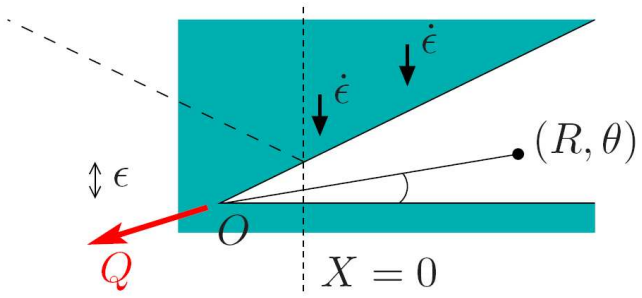

Figure 4: Diagram and notation for flow in a corner. The dashed line illustrates the outline of the wedge in Figure 3, and the symmetry axis $X = 0$.

as $\epsilon \to 0$. This suggests that the wedge will make contact with the horizontal surface at the finite time $t = t_1$ (here a constant dependent upon the initial conditions), suggesting that sharp edges might be a way to achieve contact in finite time. However, since the lubrication approximation can not be expected to hold near the vertex $X = 0$, we aim to verify this conclusion by constructing a more reasonable approximation to the Stokes equations.

2.1.2 Outer Stokes solution

We now aim to determine an approximation to the Stokes flow beneath the wedge by considering the similar problem of flow in a corner, as illustrated by Figure 4. We aim to find the Stokes flow in a corner of angle α, with velocity boundary conditions corresponding to those in the falling wedge problem. In polar coordinates (R, θ) with the origin indicated, we define a streamfunction $\psi(R, \theta)$ such that $u_R = R^{-1}\partial_\theta \psi$ and $u_\theta = -\partial_R \psi$, write the Stokes equations and boundary conditions in the form

$$\nabla^4 \psi = 0 \quad \text{in } 0 < \theta < \alpha \tag{11}$$

$$\psi(R, 0) = \frac{\partial \psi}{\partial \theta}(R, 0) = 0 \tag{12}$$

$$\frac{\partial \psi}{\partial R}(R, \alpha) = -\cos\alpha \tag{13}$$

$$\frac{\partial \psi}{\partial \theta}(R, \alpha) = R\sin\alpha. \tag{14}$$

The boundary conditions (12-14) simply represent the no-slip conditions $\mathbf{u} = 0$ on $\theta = 0$ and $\mathbf{u} = \dot{\epsilon}\hat{\mathbf{z}}$ on $\theta = \alpha$ in dimensionless variables. As stated, this biharmonic problem does not have a unique solution. If we insist that the velocity be bounded as $R \to \infty$ then we could expect to find a solution of the form

$$\psi(R, \theta) = f(\theta) + Rg(\theta). \tag{15}$$

The R-independent term in (15) will correspond to a line source or sink located at the origin. This term is not necessary when aiming to find a solution to the equations (11-14),

but has been included as a means of matching up the volume fluxes in this corner flow problem with those expected in the falling wedge problem. By symmetry, we expect that there will be no horizontal volume flux through $X = 0$ in the falling wedge. In this problem we recreate this boundary condition by selecting the strength Q of the sink at the origin so that there is no flux through $R = \epsilon/\sin\alpha$. In other words, we add the additional boundary condition

$$\psi\left(\frac{\epsilon}{\sin\alpha}, \theta\right) = 0 \tag{16}$$

to the equations (11-14). The equations can then be solved easily to yield the solutions

$$f(\theta) = \epsilon\cot\alpha\left[(\cos 2\alpha - 1)(\cos 2\theta - 1) + \sin 2\alpha(\sin 2\theta - 2\theta)\right], \tag{17}$$

$$g(\theta) = \frac{(\alpha + \sin\alpha\cos\alpha)(\theta\cos\theta - \sin\theta) + \theta\sin^2\alpha\sin\theta}{\sin^2\alpha - \alpha^2}. \tag{18}$$

It should be noted that this solution is *not* an exact solution for flow beneath the falling wedge discussed earlier. In particular, it does not allow for the streamfunction to be antisymmetric about the vertex of the falling wedge. However, it obeys all of the same boundary conditions away from the vertex of the wedge, so should be an outer solution, valid further than an $\mathcal{O}(\epsilon)$ distance from the vertex. It is essentially the leading-order contribution to the streamfunction in the limit $\epsilon \to 0$. Note also that this approximation is valid for arbitrary inclination α, unlike the lubrication approximation discussed in §2.1.1. Indeed, as $\alpha \to \pi/2$, this solution will exactly recreate the asymmetry needed at $X = 0$ in the falling wedge problem.

Having obtained this solution, we could consider the resistive force that the associated fluid flow should exert on the boundary ($R > \epsilon/\sin\alpha, \theta = \alpha$), corresponding to half of the wedge in Figure 3. As we expect the horizontal component of this force to vanish by symmetry, we consider only the vertical force on the whole wedge, namely

$$F_Z = 2\int_{\epsilon/\sin\alpha}^{1/\cos\alpha + \epsilon\sin\alpha} \hat{\mathbf{z}}\cdot\sigma\cdot\mathbf{n}\,\mathrm{d}R, \tag{19}$$

$$= 2\left[(g + g'')\sin\alpha + (g' + g''')\cos\alpha\right]\log\left(\frac{\epsilon}{\sin\alpha}\right) + 2\left[f''\sin\alpha + (f' + f''')\cos\alpha\right] + \mathcal{O}(\epsilon), \tag{20}$$

where the various derivatives of f and g are evaluated at $r = \alpha$. Substituting for these using the expression (17-18), we find that the vertical force is given by

$$F_Z = 2\left(\frac{2\alpha + \sin 2\alpha}{\alpha^2 - \sin^2\alpha}\right)\log\left(\frac{\epsilon}{\sin\alpha}\right) - 8\cos\alpha(1 + \cos^2\alpha) + \mathcal{O}(\epsilon). \tag{21}$$

Considering only the leading-order term, we can set this equal to the weight of the wedge and restore dimensions to find that, according to this solution

$$\epsilon\log\epsilon \sim \frac{Mg'(\sin^2\alpha - \alpha^2)}{2\mu L(2\alpha + \sin 2\alpha)}(t_2 - t), \tag{22}$$

as $\epsilon \to 0$. Once again, the wedge will make contact with the horizontal plane in finite time, at $t = t_2$. It is very interesting to note that we obtain the same functional form as in (10),

which was obtained by lubrication theory. Furthermore, the prefactors in equations (10) and (22) have the same leading-order behaviour for $\alpha \ll 1$. This seems to be an encouraging sign that finite-time contact may be possible even with the full Stokes equations, but we must note that this outer solution does not correctly describe the flow in the vicinity of the sharp point. In order to fully demonstrate that finite-time contact *is* possible with this sharp wedge we must resort to a full, numerical solution of the Stokes equations.

2.1.3 Full Stokes solution

In this section, we obtain a numerical solution for the streamfunction $\psi(x, z)$ describing the Stokes flow beneath the falling wedge of Figure 3. For conditions on the vertical boundaries, we use the antisymmetry of ψ at $X = 0$, and match to the outer solution (15,17,18) at the edge of the wedge. We therefore solve the biharmonic problem

$$\nabla^4 \psi = 0 \quad \text{in } -1 < X < 1, 0 < Z < H(X) \tag{23}$$

$$\psi(X,0) = \frac{\partial \psi}{\partial Z}(X,0) = \frac{\partial \psi}{\partial X}(X, H(X)) = 0, \tag{24}$$

$$\frac{\partial \psi}{\partial X}(X, H(X)) = -1, \tag{25}$$

$$\psi(X, Z) = -\psi(-X, Z), \tag{26}$$

$$\psi(1, Z) = \psi_{\text{outer}}(1, Z), \tag{27}$$

where $\psi_{\text{outer}}(X, Z)$ is the outer solution given by (15,17,18), using the coordinate transformation

$$R = \sqrt{(X + \epsilon \cot \alpha)^2 + Z^2}, \qquad \theta = \tan^{-1}\left(\frac{Z}{X + \epsilon \cot \alpha}\right). \tag{28}$$

The asymmetry constraint (26) both allows us to consider only the region $0 < X < 1$, and provides boundary conditions on the streamfunction at $X = 0$

Our numerical solution of equations (23-28) was performed by first mapping the region onto the unit square, via the transformation

$$\xi = X, \qquad \zeta = \frac{Z}{H(X)}, \tag{29}$$

and transforming the equations and boundary conditions accordingly. It is then a simple matter to discretise the equations on a uniform (ξ, ζ) grid by using a second-order finite difference scheme. The numerical solution then becomes a simple linear system, which can be inverted either exactly via LU factorization, or approximately by an iterative method that takes advantage of the sparsity of the matrix defining the problem.

After testing the code by using several exact solutions of the biharmonic equation, and confirming that the error decreases as $\mathcal{O}(\Delta X^2)$, we were able to calculate the streamfunction (and hence the velocity field) for a variety of angles α. Two examples are shown in Figure 5. Observe that, for smaller angles ($\alpha = \pi/12$ in Figure 5), the horizontal velocity field exhibits the parabolic shape (5), as obtained under the lubrication approximation, throughout most of the domain. For a sharper wedge ($\alpha = \pi/3$ in Figure 5), the horizontal velocity is concentrated more towards the horizontal surface, more like the outer solution described

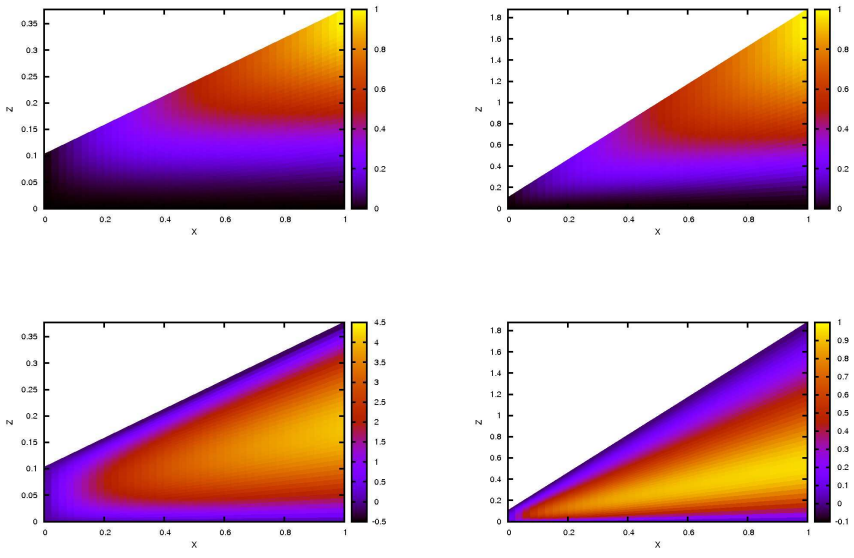

$\alpha = \pi/12$ $\alpha = \pi/3$

Figure 5: Plot of the streamfunction ψ and horizontal velocity $U = \partial_Z \psi$ beneath the falling wedge for $\alpha = \pi/12$ and $\alpha = \pi/3$. Note that $\epsilon = 0.1$ in both cases.

in §2.1.2. Both examples shown here indicate, therefore, that the approximate solutions considered previously can reasonably represent the main features of the flow for large and small α, respectively.

Given the streamfunction and velocity field, we can calculate the pressure and stress fields, allowing us to compute the vertical force acting on the wedge

$$F_Z = \int \hat{\mathbf{z}} \cdot \sigma \cdot \mathbf{n} \, \mathrm{d}S \tag{30}$$

$$= \int_{-L}^{L} \left[\cos\alpha \left(P - \frac{\partial U}{\partial X} \right) + \frac{1}{2} \sin\alpha \left(\frac{\partial U}{\partial Z} + \frac{\partial V}{\partial X} \right) \right]_{Z=H(X)} \mathrm{d}X \tag{31}$$

$$= 2 \int_{0}^{L} \left[-\cos\alpha \left(X \frac{\partial P}{\partial X} + \frac{\partial U}{\partial X} \right) + \frac{1}{2} \sin\alpha \left(\frac{\partial U}{\partial Z} + \frac{\partial V}{\partial X} \right) \right]_{Z=H(X)} \mathrm{d}X, \tag{32}$$

after integrating by parts, using the pressure boundary condition $P(\pm L) = 0$, and observing that all of the quantities in the integrand are even functions of X. Plots of the vertical force as a function of ϵ are shown in Figure 6. We observe that, in both the case of a relatively bluff wedge ($\alpha = \pi/12$) and a relatively sharp wedge ($\alpha = \pi/3$), the small ϵ behaviour of the force is a linear function of $\log\epsilon$, as predicted by our analytical results. Furthermore, the slope of this linear function agrees well with that predicted by the outer solution in both cases. However, in the small-α case, the lubrication solution (8) provides a better prediction of the constant term that forms the first correction. In the high-α example, the force predicted by the outer solution matches the numerical force extremely closely, but

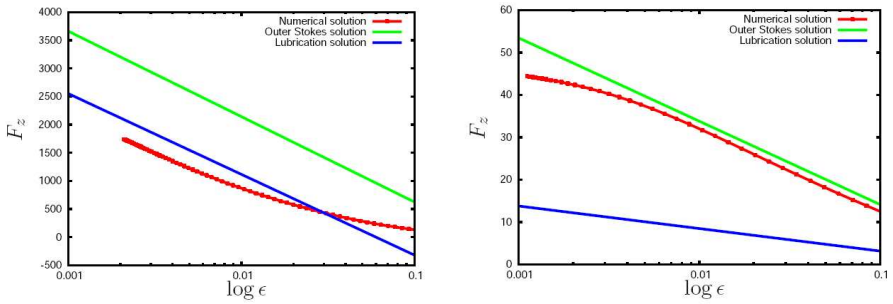

Figure 6: Plots of the vertical force F_Z, as determined by lubrication theory (8), the outer Stokes solution (21), and the numerical solution, via (32). First-order (constant) corrections have been included in the asymptotic results. Two wedge angles ($\alpha = \pi/12$ and $\alpha = \pi/3$) are shown.

it should be noted that the agreement between numerical and analytical results degrades as ϵ becomes very small. We believe that this represents a problem with the numerical resolution of our numerical scheme when the separation ϵ is very small. In this limit, the transformation (29) is near-singular in the vicinity of $X = 0$, so we should expect to need to use a higher spatial resolution in this region. This remains as potential future work.

To conclude our discussion of this problem, we make two important assertions. Firstly, both our analytical and numerical results support the hypothesis that objects with sharp asperities can make contact with a smooth surface in finite time. This suggests that roughness may indeed be an important consideration in determining settling dynamics at small lengthscales. However, one could argue that no physical surface is perfectly rough, and must be rounded on some lengthscale. Some preliminary numerical experiments with a rounded wedge were carried out, and the behaviour of the vertical force examined. For relatively large separations, the effect of rounding the corner is negligible, and the force remains proportional to $\log \epsilon$ for moderate ϵ. However, for very small lengthscales (on the order of the amount by which the corner was rounded), we observe that the force scales algebraically with ϵ. In other words, the pressure force from beneath the smoothed corner is large enough to dominate the logarithmic behaviour that arises due to the straight-edged wedge.

The second statement that we make is that, in this case at least, lubrication theory predicts the correct functional dependence of the vertical force on the minimum separation ϵ, though it is quantitatively incorrect for larger angles, as we should expect. This seems to suggest that any corrections made to the flow field due to considering the full Stokes equations are mere details that do not qualitatively affect the settling dynamics of sharp objects. For the remainder of this document, we shall use this result to justify the use of only lubrication theory in the following calculations.

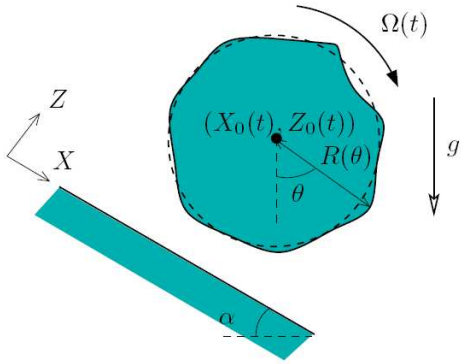

Figure 7: Diagram and (dimensionless) notation for the rough cylinder problem.

2.2 Motion of a rough cylinder

We now turn our attention to a different problem involving the effect of roughness on settling. We aim to investigate the effect of asperities on an object that is able to rotate as it settles. Should an object fall preferentially with its sharp edges pointing downwards, or will it orientate itself in such a was as to make the roughness less significant? In order to attempt to answer this question, we consider the model problem of a rough, solid cylinder settling on an inclined plane under the influence of gravity in a viscous fluid, as shown in Figure 7.

In our set-up of the problem, the cylinder has a radius

$$r(\theta) = R_0 R(\theta) = R_0 \left[1 + \eta(\theta)\right] \tag{33}$$

where θ is the polar angle measured relative to the normal to the inclined plane, as shown. The centre of the unperturbed cylinder is located at $(x_0(t), z_0(t))$, measured in Cartesian coordinates parallel and perpendicular to the plane, respectively. The rigid body motion of the cylinder can therefore be described by a translational velocity $(\dot{x}_0, \dot{z}_0)$ and an angular velocity ω measured about this centre point. The plane itself is inclined at angle α to the horizontal, and the cylinder has effective mass $M'g$. We also define Cartesian coordinates (x, z) to be locally parallel and perpendicular to the inclined plane, with the line $x = 0$ passing through the centre of the undisturbed cylinder.

2.2.1 Governing equations

In order to describe the motion of the rough cylinder, we aim to calculate the hydrodynamic force and torque acting on the cylinder, each as a function of the rigid-body motion of the cylinder. We assume that the Reynolds number of the flow is sufficiently small to allow us to apply the Stokes equations. Linearity will then imply that we can express these functions as a linear system of the form

$$(F_X, F_Z, G)^T = \mathbf{M}(\dot{x}_0, \dot{z}_0, \omega)^T$$

where $\mathbf{F} = (F_X, F_Z)$ is the force, and G the torque exerted on the cylinder by the fluid. $\mathbf{M}$ is a resistance matrix expressing the effect of geometry on the linear system. We aim to construct $\mathbf{M}$ by assuming that the dominant contributions to both the force and torque come from the thin gap between the cylinder and the plane, and applying the lubrication approximation in this gap. Even for 'sharp' roughness, the results of §2.1 suggest that this approximation will not qualitatively change the dynamics of the cylinder when compared with a full Stokes solution under the cylinder. By then making a quasi-stationary approximation, reflecting the instantaneity of Stokes flow, we equate the hydrodynamic force and torque to those exerted by gravity, and solve for the velocity and angular velocity of the current configuration by inverting the resistance matrix $\mathbf{M}$. Before proceeding with the derivation of $\mathbf{M}$, we nondimensionalise the physical variables by writing

$$(x, z, x_0, z_0) = R_0(X, Z, X_0, Z_0), \qquad (u, \dot{X}_0, \dot{Z}_0) = \frac{M'g}{\mu}(U, \dot{X}_0, \dot{Z}_0), \qquad (\omega, t^{-1}) = \frac{M'g}{\mu R_0}(\Omega, T^{-1}).$$

In order to use the lubrication solution in the Cartesian coordinates (X, Z), we must first express the thickness $H = h/R_0$ of the gap beneath the cylinder as a function of the downslope coordinate X. A simple geometrical calculation leads to the relationship

$$X = [1 + \eta(\theta - \phi)] \sin\theta, \tag{34}$$

where $\phi = \int \Omega \, \mathrm{d}T$ describes the current orientation of the cylinder. The gap thickness can then be expressed as

$$H(X) = Z_0 - (1 + \eta(\theta - \phi)\cos\theta) = Z_0 - \sqrt{(1 + \eta(\theta - \phi))^2 - X^2} \tag{35}$$

Assuming that the roughness $\eta \ll 1$, we approximate the relationship (34) by taking $\theta = \sin^{-1} X$ in (35).

As is usual for lubrication flows, the horizontal velocity profile will be parabolic, and of the form

$$U(X, Z) = V\frac{Z}{H(X)} - \frac{1}{2}\frac{\partial P}{\partial X} Z\left(H(X) - Z\right), \tag{36}$$

where V is the horizontal velocity at $Z = H(X)$, given by

$$\begin{aligned} V &= \dot{X}_0 + \Omega\left[1 + \eta(\theta - \phi)\right]\cos\theta, \\ &= \dot{X}_0 + \Omega\sqrt{(1 + \eta(\theta - \phi))^2 - X^2}, \\ &= \dot{X}_0 + (Z_0 - H)\Omega \end{aligned} \tag{37}$$

By integrating the continuity equation in Z, we find that

$$\frac{\partial}{\partial X}\left(\int_0^{H(X)} U \, \mathrm{d}Z\right) - \frac{\partial H}{\partial X} V + W = 0, \tag{38}$$

where W is the vertical velocity at $Z = H(X)$, namely

$$\begin{aligned} W &= \dot{Z}_0 + \Omega\left[1 + \eta(\theta - \phi)\right]\sin\theta, \\ &= \dot{Z}_0 + X\Omega \end{aligned} \tag{39}$$

By combining equations (36-39), we arrive at the Reynolds equation

$$\frac{\partial}{\partial X}\left[-\frac{H^3}{12}\frac{\partial P}{\partial X}-\frac{1}{2}H\dot{X}_0+X\dot{Z}_0+\frac{1}{2}\left(X^2-Z_0H\right)\Omega\right]=0. \tag{40}$$

After taking a first integral of (40), we use the boundary condition $P(\pm1)=\int_{-1}^{1}\partial_X P\,\mathrm{d}X=0$, to determine the constant of integration and express the pressure gradient in the form

$$\frac{\partial P}{\partial X}=\frac{6}{H^3 I_{03}}\left[\dot{X}_0\left(I_{02}-HI_{03}\right)+2\dot{Z}_0\left(XI_{03}-I_{13}\right)+\Omega\left(X^2I_{03}-I_{23}+Z_0I_{02}-Z_0HI_{03}\right)\right], \tag{41}$$

where the constants I_{mn} are defined by the integrals

$$I_{mn}=\int_{-1}^{1}\frac{X^m}{H(X)^n}\,\mathrm{d}X. \tag{42}$$

Having obtained expressions for the velocity field (36) and pressure gradient (41), we can proceed to find the force and torque on the rough cylinder. The force is given by

$$\begin{aligned}\frac{\mathbf{F}}{M'g}=\frac{(F_X,F_Z)}{M'g}&=\int\sigma\cdot\mathbf{n}\,\mathrm{d}S\\&=\int_{-1}^{1}\left(\left\{-P+\frac{\partial U}{\partial X}\right\}\frac{\partial H}{\partial X}-\frac{1}{2}\frac{\partial U}{\partial Z},P\right)\mathrm{d}X+\mathcal{O}\left(\left[\frac{\partial H}{\partial X}\right]^2\right)\\&=\int_{-1}^{1}\left(\frac{3H}{4}\frac{\partial P}{\partial X}-\frac{Z_0}{2H}\dot{X}_0+\frac{\Omega}{2},-X\frac{\partial P}{\partial X}\right)\mathrm{d}X+\mathcal{O}\left(\left[\frac{\partial H}{\partial X}\right]^2\right).\end{aligned} \tag{43}$$

We neglect the higher order terms in accordance with the lubrication approximation. Substituting for the pressure gradient using (41), we can express the force on the cylinder as

$$\frac{\mathbf{F}}{6M'g}=(M_{11}\dot{X}_0+M_{12}\dot{Z}_0+M_{13}\Omega,M_{21}\dot{X}_0+M_{22}\dot{Z}_0+M_{23}\Omega), \tag{44}$$

where

$$M_{11}=\tfrac{3}{4}\left(I_{02}^2-\tfrac{2}{3}I_{01}I_{03}\right)/I_{03}, \tag{45}$$
$$M_{12}=\tfrac{3}{2}\left(I_{03}I_{12}-I_{13}I_{02}\right)/I_{03}, \tag{46}$$
$$M_{13}=\left[\tfrac{1}{6}I_{03}+\tfrac{3}{4}(I_{03}I_{22}-I_{23}I_{02})+\tfrac{3}{4}Z_0(I_{02}^2-\tfrac{8}{9}I_{01}I_{03})\right]/I_{03}, \tag{47}$$
$$M_{21}=(I_{02}I_{13}-I_{03}I_{12})/I_{03}, \tag{48}$$
$$M_{22}=2(I_{03}I_{23}-I_{13}^2)/I_{03}, \tag{49}$$
$$M_{33}=\left[I_{03}I_{33}-I_{13}I_{23}-Z_0(I_{03}I_{12}-I_{02}I_{13})\right]/I_{03}. \tag{50}$$

The torque about the centre of the unperturbed cylinder is given by

$$\begin{aligned}\frac{G}{M'gR}&=\int(1+\eta)\mathbf{t}\cdot\sigma\cdot\mathbf{n}\,\mathrm{d}S,\\&=\int_{-1}^{1}\frac{1+\eta(\theta-\phi)}{2}\frac{\partial U}{\partial Z}\,\mathrm{d}X,\\&=\frac{1}{4}\int_{-1}^{1}\sqrt{X^2+(Z_0-H)^2}\left\{H\frac{\partial P}{\partial X}+2\frac{\dot{X}_0}{H}+\frac{2(Z_0-H)\Omega}{H}\right\}\mathrm{d}X.\end{aligned} \tag{51}$$

In obtaining (51), we have used the expression for H (35) to remove the explicit dependence on the roughness η. After substituting for the pressure gradient using (41) and evaluating the integrals, we find the the torque can be written in the form

$$\frac{G}{M'gR} = M_{31}\dot{X}_0 + M_{32}\dot{Z}_0 + M_{33}\Omega, \tag{52}$$

where

$$M_{31} = (\tfrac{3}{2}I_{02}J_{02} - I_{03}J_{01})/I_{03}, \tag{53}$$
$$M_{32} = 3(I_{03}J_{12} - I_{13}J_{02})/I_{03}, \tag{54}$$
$$M_{33} = \left[-\tfrac{1}{2}I_{03}J_{00} + \tfrac{3}{2}(I_{03}J_{22} - I_{23}J_{02}) - Z_0(I_{03}J_{01} - \tfrac{3}{2}I_{02}J_{02})\right]/I_{03}. \tag{55}$$

Here, the coefficients J_{mn} are defined by

$$J_{mn} = \int_{-1}^{1} \sqrt{X^2 + (H - Z_0)^2}\frac{X^m}{H^n}\,\mathrm{d}X. \tag{56}$$

This completes our derivation of the resistance matrix $\mathbf{M}$, which is defined by its components (45-50) and (53-55). Given the force and torque acting on the cylinder, we can invert M to find the velocity and angular velocity, provided that $\mathbf{M}$ is nonsingular.

2.2.2 Free cylinder

For the physically important problem of settling along an inclined plane under gravity, we assume that the roughness is sufficiently small that we may neglect any gravitational torque. We therefore set $G = 0$, $F_X = M'g\sin\alpha$, and $F_Z = M'g\cos\alpha$ to find that

$$\dot{X}_0 = \frac{M'g}{\det(M)}\left[\sin\alpha(M_{22}M_{33} - M_{12}M_{21}) + \cos\alpha(M_{13}M_{32} - M_{12}M_{23})\right], \tag{57}$$
$$\dot{Z}_0 = \frac{M'g}{\det(M)}\left[\sin\alpha(M_{23}M_{31} - M_{21}M_{33}) + \cos\alpha(M_{11}M_{13} - M_{31}M_{13})\right], \tag{58}$$
$$\Omega = \frac{M'g}{\det(M)}\left[\sin\alpha(M_{21}M_{32} - M_{31}M_{22}) + \cos\alpha(M_{13}M_{21} - M_{11}M_{23})\right]. \tag{59}$$

It should be noted that all of the coefficients M_{ij} depend upon two parameters, namely the current height Z_0 and the current orientation ϕ. The equations (57-59) therefore define an autonomous ordinary differential equation for the position and orientation of the cylinder as a function of time. Note also that the evolution of the downslope position is slaved to the height and orientation.

In order to investigate the behaviour of the system (57-59), we consider a sample roughness function in the form of a sawtooth with m teeth – i.e. a periodic function

$$\eta(\theta) = \eta\left(\theta + \frac{2n\pi}{m}\right) = A\theta, \quad -\frac{\pi}{m} < \theta < \frac{\pi}{m}, \quad n = \pm 0, \pm 1, ..., \pm(m-1). \tag{60}$$

The results presented here are for $m = 10$, but we shall discuss other values of m at the end of this subsection.

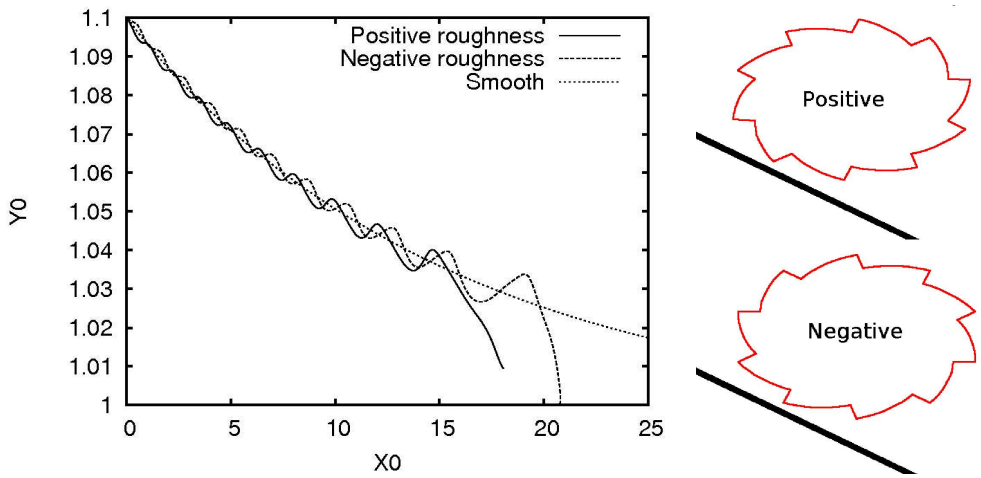

Figure 8: Trajectory of the centre of mass (X_0, Z_0) of a rough cylinder falling freely down a plane inclined at angle $\alpha = \pi/6$. Positive and negative roughness corresponds to the sawtooth roughness function (60) with $m = 10$ and $A = \pm 0.01$ respectively.

Figure 8 shows the trajectories described by the centre of the cylinder (X_0, Z_0) in typical numerical simulations. For comparison, we also show the trajectory of a smooth cylinder under the same conditions. We see that the paths of the rough and smooth cylinders are largely similar. When far from the inclined plane, the path of the rough cylinder oscillates about the path of the smooth cylinder. For 'positive' roughness, periods of gradual ascent are interspersed by shorter periods of relatively rapid descent. For 'negative' roughness, we observe short periods of ascent interrupting longer periods of gradual descent. In both cases, however, there is a net decrease in height over these two intervals.

Given the absence of such oscillations in the case of a smooth cylinder, the only cause can be the addition of the symmetry-breaking roughness to the cylinder. In fact, the longer periods of gradual ascent or enhanced descent can be explained by the sawteeth acting as Reynolds bearings as illustrated in Figure 9. In each case, gravity forces the cylinder to move downslope. For negative roughness, the local geometry of a tooth moving past the inclined plane resembles that of a Reynolds bearing (Figure 9a), where hydrodynamical forces in the converging channel generate a net lift force on the cylinder. For positive roughness, the situation is reversed (Figure 9b), and the net hydrodynamical force on the cylinder is directed towards the plane. When added to the resistive pressure force that comes from squeezing out fluid from beneath the cylinder, this bearing effect can either oppose or enhance the settling of the cylinder due to gravity.

However, gravity also exerts a torque on the cylinder, forcing to it to rotate so that the Reynolds bearing/antibearing geometry changes to one in which a sharp tooth is near the base of the cylinder. This gives rise to the shorter periods of motion in the opposite direction. In the case of positive roughness, the passing of the tooth abruptly increases the thickness of the gap between the cylinder and the plane, reducing the resistive forces and allowing for an increased settling velocity. For negative roughness, the sharp decrease in the

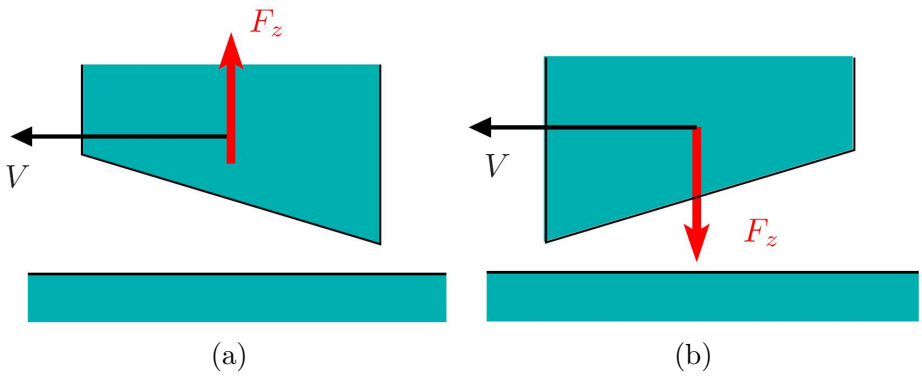

Figure 9: Cartoon of Reynolds bearings. (a) If the fluid moves towards a narrowing gap, a lift force is generated. (b) If fluid moves towards an expanding gap, a suction force arises.

gap thickness results in a short-lived upward force, and allows the cylinder to rise slightly before settling once again into the falling part of the cycle.

Whether the roughness is in the form of a positive or negative sawtooth, the end result is essentially the same. When the cylinder comes close enough to the plane, the gravitational torque is insufficient to keep the cylinder rolling downslope, and it gets stuck with a sharp point near its base. The numerical results seem to suggest that contact in finite time then follows (though it is difficult to distinguish finite-time contact from a finite-time approach predicted by a numerical scheme with too large a timestep). However, we could believe, given the results of §2.1, that the sharp corner does allow finite-time contact.

The above discussion applied for $m = 10$. If we change m, the number of teeth on the rough cylinder, the results remain qualitatively unchanged. In each case, it seems that the the cylinder will reach contact in finite time, and its trajectory oscillates around that of a smooth cylinder until it comes sufficiently close to the inclined plane, at which point rotation is arrested and the sharp corner can begin to effect finite-time settling.

After the preparation of an early form of this report, a paper by Zhao *et al.*[6] was brought to our attention. In this paper, the authors investigate experimentally the rolling of a smooth sphere down an inclined plane of carefully-controlled roughness. They look in detail at the dynamics of the sphere as it passes over an asperity, and use a similar lubrication model to describe them. We direct the interested reader to [6] for a much more detailed and polished version of the above analysis.

2.2.3 Driven cylinder

As a brief aside, we draw attention to the dynamics of a roughened cylinder forced to rotate at constant (dimensionless) angular velocity Ω_0, but that is otherwise free to move. In order to allow for comparison with the case of a free cylinder, we use the same definitions of positive and negative roughness (i.e. the sawtooth roughness of (60) with $m = 10$ and $A = \pm 0.1$). We present here results for zero inclination angle $\alpha = 0$, but will mention the effect of varying α at the end of this subsection. The restriction of the free cylinder problem to a driven problem can be achieved under the previous resistance matrix framework by

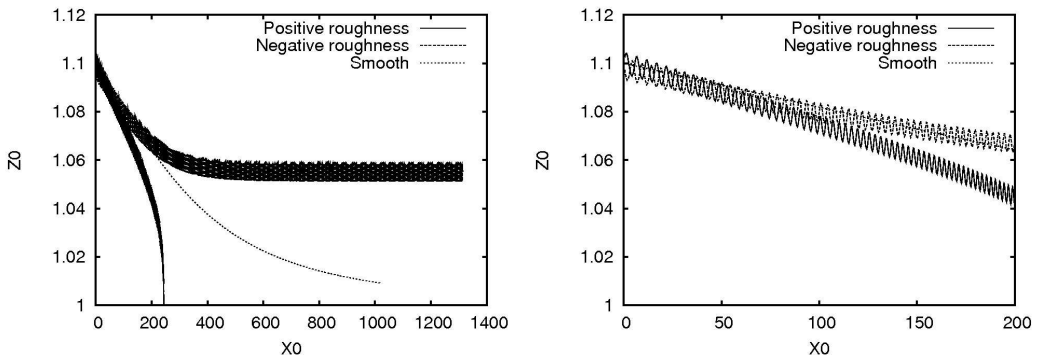

Figure 10: Trajectories of a driven cylinder falling down an inclined plane. Positive and negative roughness correspond to the sawtooth roughness (60) with $m = 10$ and amplitude $A = \pm 0.1$. The plane beneath the cylinder is horizontal – $\alpha = 0$. The trajectory of a smooth cylinder is shown for comparison. The second graph shows a magnification of the initial region $0 < X_0 < 200$, showing detail of the ratchet-like motion.

setting $M_{31} = M_{32} = 0$, $M_{33} = 1$, and $G = \Omega_0$. Figure 10 shows the trajectories followed by the centre of mass of the cylinder in the cases of positive and negative roughness, where the cylinder is driven in a clockwise sense.

In the case of positive roughness, we see that the cylinder rapidly descends towards the horizontal plane, and appears (numerically) to make contact in finite time. This can be explained in a similar manner to the apparent finite-time contact observed for the free cylinder. In this case, however, the settling is greatly accelerated by the rotation of the cylinder, which generates a strong suction force via Reynolds anti-bearing action (Figure 9b).

In the case of negative roughness, however, we observe that, following an initial period where the cylinder settles at a (time-averaged) rate similar to that of a smooth cylinder, the vertical position of the centre of mass, Z_0 tends to a stable periodic oscillation about the value $Z_0 \approx 1.05$. In other words, the cylinder will remain suspended above the plane indefinitely, as long as it continues to be driven to rotate. The existence of this suspended state is quite robust to variation of the rotation rate and roughness parameters, though the limiting mean value of Z_0 decreases as the rotation rate, roughness amplitude, and number of teeth decrease.

In both of the above cases, looking more closely at the trajectories reveals a ratchet-like behaviour, similar to the case of a free rough cylinder, where longer periods of gradual rise or fall are interspersed with short periods of motion in the opposite direction. However, in this case, it is the act of driving the cylinder that produces horizontal motion, rather than gravity. If the cylinder rotates fast enough in the appropriate direction for the roughness, then it can provide sufficient lift (during those intervals when we have a Reynold bearing geometry) for the net change in height during the passing of one tooth to be zero at some critical height. This gives rise to the periodic oscillation observed here for negative roughness.

Varying the inclination angle does little to change the qualitative dynamics of the driven system. A fairly coarse search of the parameter space indicates that the suspended state

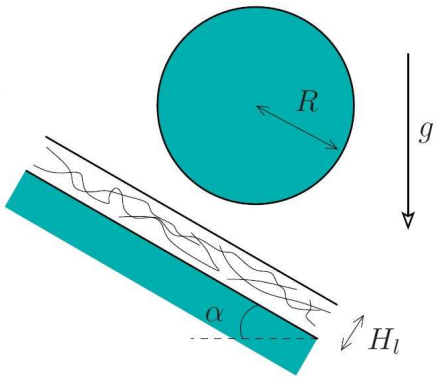

Figure 11: Diagram and notation for elastic lubrication problem

still exists for any angle, provided that the sense of the rotation is correct. For a large enough angle, it may be the case that the downslope component of force can balance the upslope component of the viscous drag due to rotation, and one could find a system in which both X_0 and Z_0 exhibit periodic oscillations. The search for such a state did not, however, form a part of the work carried out during the GFD Program.

3 Elasticity

The infinite contact time predicted by a simple lubrication model requires the appearance of very large fluid pressures when the gap between the falling object and the substrate are very small. It is quite possible that these large pressures could cause some small deformation of the solid surfaces, which were previously assumed to be rigid. It is not immediately obvious whether elastic effects should aid or oppose settling. In this section, we develop ideas proposed by Skotheim & Mahadevan [4] about lubrication films between elastic layers, and attempt to apply them to settling problems.

3.1 Lubrication with elastic layers

We consider a situation such as that shown in Figure 11. A smooth cylinder of radius R is settling under gravity towards an smooth plane, inclined at angle α to the horizontal, that is coated with a thin layer of thickness H_l of an elastic material. We define a local Cartesian coordinate system (x, z) to be aligned with the inclined plane, and take $x = 0$ to pass through the centre of the cylinder.

We assume that the elastic material has a linear, isotropic stress-strain relationship, with stress tensor

$$\sigma_e = G(\nabla \mathbf{u} + (\nabla \mathbf{u})^T) + \lambda(\nabla \cdot \mathbf{u})\mathbf{I}, \tag{61}$$

where $\mathbf{u}$ is the local displacement vector, $\mathbf{I}$ is the identity tensor, and G and λ are Lamé coefficients describing the elasticity of the medium. The elastic problem to be solved,

assuming a quasi-steady state, is

$$\nabla \cdot \sigma_{\mathbf{e}} = 0 \tag{62}$$

$$\mathbf{u}(X, -H_l) = \mathbf{0} \tag{63}$$

$$\sigma_e \cdot \mathbf{n} = -p\mathbf{n} \quad \text{at } z = u_z(x, 0) \tag{64}$$

which corresponds to a local force balance, with no displacement allowed on the lower boundary, and continuity of stress on the surface in contact with the fluid. If we assume that the layer is thin compared to the horizontal extent of the lubrication film, then we can proceed in the same manner as fluid lubrication, by neglecting horizontal variations when determining the displacement field. We therefore approximate (62) by

$$(2G + \lambda)\frac{\partial^2 u_z}{\partial z^2} = 0,$$

giving us the approximate solution

$$u_z(x, z) \approx -\frac{p(x)}{2G + \lambda}(z + H_l). \tag{65}$$

The size of the fluid-filled gap between the settling object and the elastic layer where the local pressure is $p(x)$ is given by

$$h(x) = h_0(x) + \frac{H_l}{2G + \lambda}p(x),$$

where $h_0(x)$ is the undeformed gap thickness. For the case of a settling cylinder, we approximate this by a parabola, leading to

$$h(x) = \epsilon R + \frac{x^2}{2R} + \frac{H_l}{2G + \lambda}p(x), \tag{66}$$

where ϵR is the minimum separation between the cylinder and the line $z = 0$.

The equations governing the fluid flow can be determined exactly as for a rigid cylinder approaching a rigid substrate. For a cylinder translating with velocity $(\dot{x}_0, \dot{z}_0)$, we find the Reynolds equation

$$\frac{\partial}{\partial x}\left[-\frac{h^3}{12\mu}\frac{\partial p}{\partial x} - \frac{h}{2}\dot{x}_0 + x\dot{z}_0\right] = 0. \tag{67}$$

The novel feature in this elastic problem is the feedback between pressure and gap thickness, as established by (66). Some consequences of this are discussed in the next few sections.

3.2 Pure shearing

The first use of the preceding theory was made by Skotheim & Mahadevan [4], who considered the case of a cylinder travelling at a fixed height past an elastic-coated plane with speed V, as illustrated by Figure 12a. In the absence of an elastic layer, the symmetry of the translating cylinder gives rise to a perfectly symmetric pressure gradient (Figure 12b), which cannot generate lift. However, the elastic layer can be deformed by the relative pressures, and is squeezed down ahead of and beneath the cylinder, as shown in Figure 12c.

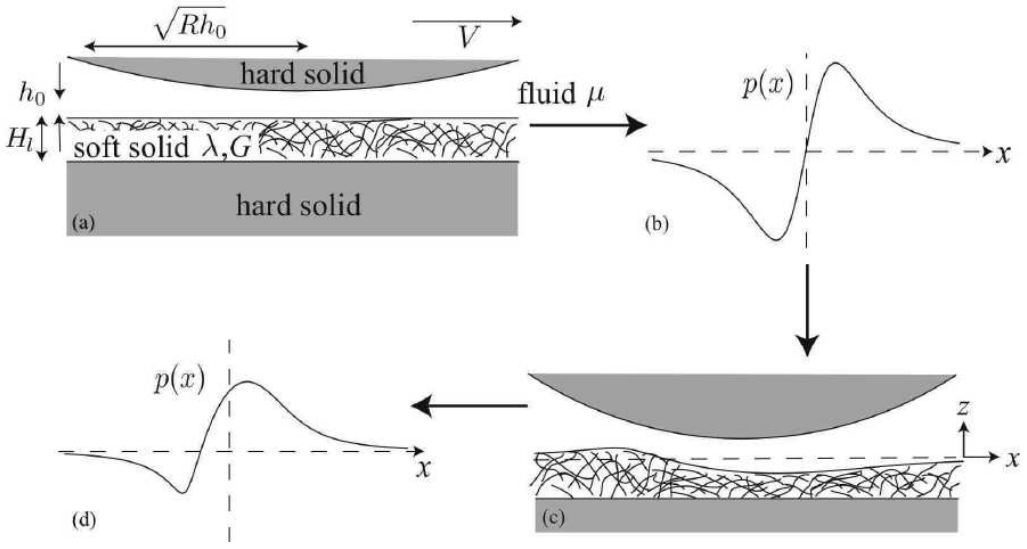

Figure 12: Illustration of how the presence of an elastic layer can generate lift. (a) A rigid object translates parallel to an elastic layer. (b) The symmetric pressure distribution that arises without elasticity. (c) Deformation of the elastic layer due to high and low relative pressures. (d) The resulting asymmetric pressure distribution. Figure copied from Skotheim & Mahadevan (2004) [4].

This in turn makes the pressure gradient asymmetric (Figure 12d), and can generate a net upward force. The mathematical details of this problem are given in full in [4], wherein the authors also consider how the lift force scales with the separation of the object from the elastic material for a range of different physical situations, including either solid object being entirely elastic and the cylinder being an elastic shell. In the context of this report, we note merely the existence of a mechanism by which the presence of elasticity in the solid bodies can generate lift, and therefore oppose the settling of an object, provided that there is some force driving the object horizontally.

3.3 Pure settling

In the absence of any horizontal forcing ($\alpha = 0$ in Figure 11), we find a situation like that shown in Figure 13. In this case, we expect that the pressure is an even function of x, and the Reynolds equation (67) can be integrated once to find that

$$\frac{\partial p}{\partial x} = \frac{12\mu R x \dot{\epsilon}}{h^3(x)}, \tag{68}$$

the constant of integration having been eliminated by integrating over $-\infty < x < \infty$ and applying the boundary conditions $p(\pm\infty) = 0$. At this point, we nondimensionalise the problem by scaling all lengths with R, time with $\mu R/M'g$, and pressure with $M'g/R$, where M'g is the effective weight per unit length of the cylinder. Substituting for the approximate gap width (66), and balancing the vertical resistive force with the effective weight of the

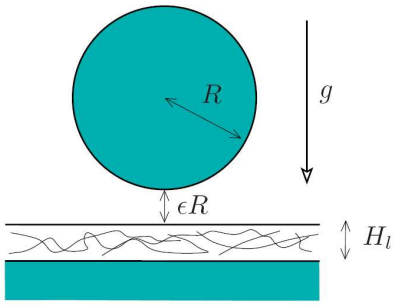

Figure 13: Diagram and notation for a vertically-settling cylinder onto an elastic layer.

cylinder, we find the the dimensionless pressure P must be a solution to the following problem

$$\frac{\mathrm{d}P}{\mathrm{d}X} = \frac{12\dot{\epsilon}X}{(\epsilon + \frac{1}{2}X^2 + \gamma P)^3}, \tag{69}$$

$$P(\pm\infty) = 0, \tag{70}$$

$$\int_{-\infty}^{\infty} P\,\mathrm{d}X = 1, \tag{71}$$

where

$$\gamma = \frac{M'gH_l}{(2G+\lambda)R^2}. \tag{72}$$

In order to solve this problem, we define the new variables ψ and ξ by

$$\xi = \epsilon^{-1/2}X, \quad \text{and} \quad \frac{\mathrm{d}\psi}{\mathrm{d}X} = \frac{\gamma P}{\epsilon}.$$

With an appropriate choice of the arbitrary constant allowed by our choice of ϕ, we transform the problem (69-71) into the second-order boundary value problem

$$\psi'' = \frac{N\xi}{(1 + \frac{1}{2}\xi^2 + \psi')^3}, \tag{73}$$

$$\psi'(\pm\infty) = 0, \tag{74}$$

$$\psi(\pm\infty) = \pm\frac{\gamma}{2\epsilon^{3/2}}. \tag{75}$$

Here $N(= 12\gamma\dot{\epsilon}/\epsilon^3)$ may be thought of as an eigenvalue for the ordinary differential equation (73) with boundary conditions (74,75). This problem can be easily solved numerically for all values of the parameter δ, resulting in the relationship between the settling speed $\dot{\epsilon}$ and the separation ϵ shown in Figure 14 Importantly, this seems to indicated that the settling velocity tends to a nonzero limit as $\epsilon \to 0$, suggesting that the cylinder *will* settle in finite time. A physical explanation for this is as follows. Deformation of the elastic film increases the mean fluid-filled gap thickness, which in turn has the result of reducing the pressure gradient (recall that the pressure gradient is proportional to h^{-3}). This results in a net

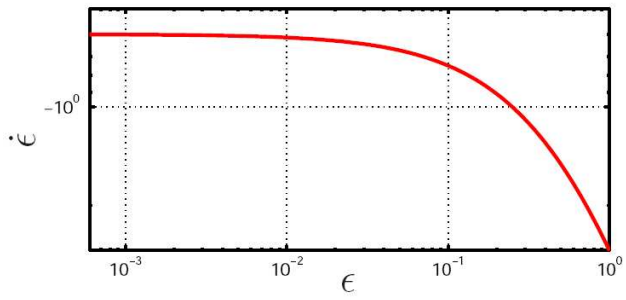

Figure 14: Graph showing the settling velocity $\dot{\epsilon}$ as a function of separation ϵ for vertical settling on to an elastic layer. Note that $\dot{\epsilon}$ tends to a finite nonzero limit as $\epsilon \to 0$.

decrease in the upward resistive force, so that $F_Z = \text{ord}(1)$ as $\epsilon \to 0$. We can understand this asymptotic behaviour analytically by defining scaled variables (ϕ, ζ) such that

$$\psi(\xi) = \frac{\gamma}{2\epsilon^{3/2}}\phi(\zeta) \quad \text{and} \quad \xi = \left(\frac{2\epsilon^{3/2}}{\gamma}\right)^{1/3} \zeta.$$

The equations (73-75) may then be expressed as

$$\frac{\mathrm{d}^2\phi}{\mathrm{d}\zeta^2} = N\left(\frac{2\epsilon^{3/2}}{\gamma}\right)^2 \frac{\zeta}{(\frac{1}{2}\zeta^2 + \frac{\mathrm{d}\phi}{\mathrm{d}\zeta} + \mathcal{O}(\epsilon))^3}, \tag{76}$$

$$\frac{\mathrm{d}\phi}{\mathrm{d}\zeta}(\pm\infty) = 0, \tag{77}$$

$$\phi(\pm\infty) = \pm 1.. \tag{78}$$

In the limit $\epsilon \to 0$, this boundary value problem can only admit solutions if the right-hand side of (73) is of order unity. That is

$$N\epsilon^3 = \text{ord}(1) \Rightarrow \dot{\epsilon} = \text{ord}(1),$$

as observed in the results of the numerical calculation described above.

This scaling for the settling velocity suggests that the addition of elasticity should allow contact in finite time, because $\epsilon \propto (t - t_0)$ for small ϵ. However, one must remember that ϵ is the height of the cylinder above the *undeformed* elastic layer. After passing through $\epsilon = 0$, the layer will simply continue to deform at a rate that maintains the ord(1) scaling for $\dot{\epsilon}$. There will come a point, of course, when the elastic layer can deform no longer, either due to nonlinear elastic effects, or the fact that deformation predicted by this simple model will exceed the thickness of the layer. At this point, we should probably expect to see the familiar $\epsilon \propto t^{-2}$ scaling for the approach of two rigid objects reappear. Our conclusion is therefore that elasticity can accelerate contact at first, but should not be able to create bona fide contact between the objects in finite time.

3.4 Arbitrary inclined plane

We now return to the situation depicted in Figure 11, where a rigid cylinder settles down an inclined plane coated with an elastic layer. In this case, the downslope component of gravity acts to drag the cylinder downhill, giving rise to a lift force as described in §3.2. Meanwhile, the perpendicular component acts to force the cylinder to settle. It is not immediately obvious which of these two effects will dominate the dynamics of the cylinder, so we shall investigate the system numerically in this section.

For simplicity, we assume that the cylinder does not rotate, and just translates with velocity $(\dot{x}_0, \dot{z}_0)$. Using the same scalings for pressure, length, time and velocity as in §3.3, the Reynolds equation (67) for the pressure gradient beneath the cylinder becomes

$$\frac{\partial}{\partial X}\left[-\frac{H^3}{12}\frac{\partial P}{\partial X} - \frac{H}{2}\dot{X}_0 + X\dot{Z}_0\right] = 0 \tag{79}$$

Vertical force balance, taken up to second order in $\partial H/\partial X$, once again requires that we equate the pressure force with the plane-perpendicular component of the weight,

$$\int_{-\infty}^{\infty} P \,\mathrm{d}X = \cos\alpha \tag{80}$$

whilst the downslope force balance becomes, after a little algebra

$$\int_{-\infty}^{\infty}\left\{\frac{\dot{X}_0}{2H} + \frac{3H}{4}\frac{\partial P}{\partial X}\right\}\mathrm{d}X = -\sin\alpha. \tag{81}$$

Along with the boundary conditions $P(\pm\infty) = 0$, equations (79-81) define a boundary value problem with two eigenvalues, namely $\dot{X}_0$ and $\dot{Z}_0$. This problem can be solved numerically by defining new dependent variables Ψ, Φ, and independent variable ξ by

$$\frac{\partial P}{\partial X} = \frac{\epsilon^{1/2}}{\gamma}\Psi'(\xi), \quad \Phi'(\xi) = \tilde{H}\Psi'' + \frac{V}{9\tilde{H}}, \quad x = \epsilon^{1/2}\xi,$$

so chosen to turn the integral constraints (80) and (81) into boundary conditions on Ψ and Φ, respectively. The scaled height $\tilde{H}$ is given by

$$\tilde{H} = 1 + \frac{1}{2}\xi^2 + \gamma P.$$

and

$$V = \frac{6\gamma\dot{X}_0}{\epsilon^{5/2}}.$$

With this transformation, we must solve the third-order boundary value problem

$$\Psi'' = \frac{A + N\xi}{\tilde{H}^3} - \frac{V}{\tilde{H}^2}, \tag{82}$$

$$\Phi' = \tilde{H}\Psi'' + \frac{V}{9\tilde{H}}, \tag{83}$$

$$\Psi(\pm\infty) = \Psi'(-\infty) = \Phi(-\infty) = 0, \tag{84}$$

$$\Psi(+\infty) = \frac{\gamma\cos\alpha}{\epsilon^{3/2}}, \tag{85}$$

$$\Phi(+\infty) = -\frac{4\gamma\sin\alpha}{3}\left(\frac{\gamma\cos\alpha}{\epsilon^{3/2}}\right)^{4/3}. \tag{86}$$

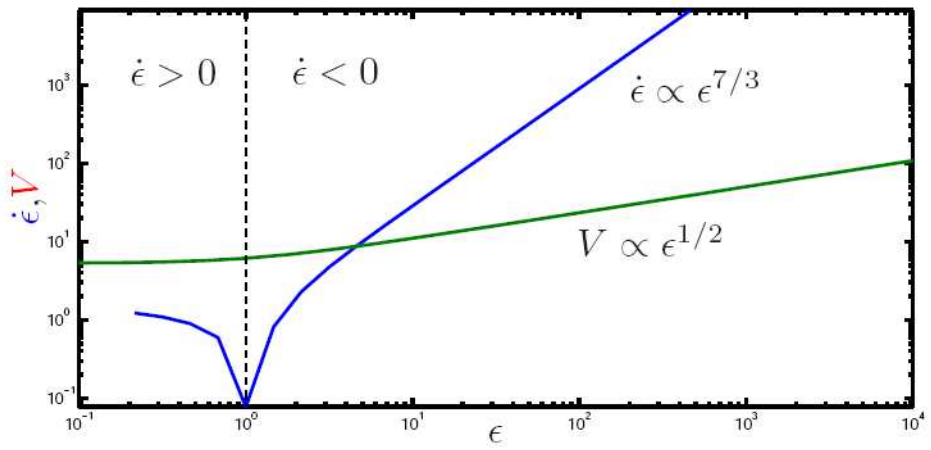

Figure 15: Log-log plot of numerical results for the eigenvalues N (in blue, compensated by ϵ^3) and V (in red, compensated by $\epsilon^{3/2}$), as a function of the separation ϵ for a cylinder falling down an elastic-coated inclined plane. Note the change in sign of N (hence $\dot{Z}_0$) in the vicinity of $\epsilon = 1$.

In equation (82), A is the constant of integration introduced when taking a first integral of the Reynolds equation (79). This must also be determined as an eigenvalue of the third-order problem, along with the quantities N and V, which relate to the settling and downslope velocities, respectively. In this problem, $N = 12\gamma\dot{Z}_0/\epsilon^3$, as in §3.3.

Solving equations (82-86) numerically, one typically finds results like those shown in Figure 15. The very important feature to note is that the eigenvalue N changes sign somewhere near $\epsilon = 1$. This suggests the existence of a (stable) steady state, where the cylinder falls down the plane at a constant velocity and constant separation from the plane. In this situation, the settling force exactly balances the lift force due to the downslope motion. Note that, unlike the driven cylinder of §2.2.3, this 'gliding' stable state exists without the need for any external forcing beyond gravity. We have also noted the apparent power-law scalings of N and V for large separations ϵ, but have not yet made an attempt to explain them physically or mathematically.

4 Compressibility

A final factor that may play a role in settling dynamics is the compressibility of the fluid film. One might expect that the high lubrication pressures could be somewhat alleviated by allowing the density of the fluid to change. With this in mind, we consider once again the problem of a settling cylinder, as illustrated in Figure 1, but this time allow for compressible effects in the fluid film.

The lubrication approximation to the equations of conservation of mass and momentum

(based on the Stokes equations) are

$$-\frac{\partial p}{\partial x} + \mu \frac{\partial^2 u}{\partial x^2} = 0, \tag{87}$$

$$\frac{\partial p}{\partial z} = 0, \tag{88}$$

$$\frac{\partial \rho}{\partial t} + \frac{\partial}{\partial x}(\rho u) + \frac{\partial}{\partial z}(\rho z) = 0. \tag{89}$$

These equations must be supplemented by an equation of state. In the case of an adiabatic gas, pressure and density are related by

$$p = K\rho^\gamma. \tag{90}$$

We also suppose that the kinematic viscosity varies with the local pressure (hence density) according to

$$\nu = Lp^m. \tag{91}$$

As in the case of an incompressible fluid, we can integrate the momentum equations (87,88) to obtain a parabolic velocity profile

$$u = -\frac{\partial_x p}{2\mu} z(h - z) \tag{92}$$

and integrate the mass conservation equation (89) in the vertical direction to find the compressible Reynolds equation

$$\frac{\partial}{\partial t}(\rho h) + \frac{\partial}{\partial x}\left(-\frac{h^3}{12\nu}\frac{\partial p}{\partial x}\right) = 0. \tag{93}$$

This equation, together with the relations (90,91) can be solved for the pressure p, subject to boundary conditions $p(\pm\infty) = 0$. Finally, we use instantaneous force balance

$$\int p \, \mathrm{d}x = Mg' \tag{94}$$

to determine the settling velocity as a function of the current shape and size of the fluid-filled gap, as in the previous sections.

Though the Reynolds equation (93) may be integrated numerically, we shall only note the existence of a late-time similarity solution. We nondimensionalise the problem by writing

$$x = RX, \qquad h = RH, \qquad p = \frac{Mg'}{R}P, \qquad t = 12L\left(\frac{Mg'}{R}\right)^{1-m-1/\gamma}.$$

After substituting for the density and kinematic viscosity, we arrive at the partial differential equation

$$\frac{\partial}{\partial T}\left(HP^{1/\gamma}\right) - \frac{\partial}{\partial X}\left(\frac{H^3}{P^m}\frac{\partial P}{\partial X}\right) = 0, \tag{95}$$

$$P(\pm\infty) = 0, \tag{96}$$

$$\int P \, \mathrm{d}X = 1 \tag{97}$$

Noting that we may approximate the gap thickness by a parabola

$$H(X,T) \approx \epsilon(T) + \frac{1}{2}X^2 = \epsilon(T)\left[1 + \frac{1}{2}\left(\frac{X}{\sqrt{\epsilon}}\right)^2\right] =: \epsilon\tilde{H}(\xi), \tag{98}$$

we aim to find a large-T similarity solution in terms of the similarity variable $\xi = X/\sqrt{\epsilon}$. By seeking a solution of the form

$$P(X,T) = T^{\lambda} f(\xi),$$

we can transform the problem (95-97) into an ordinary differential equation for in ξ only provided that

$$\frac{\dot{\epsilon}}{\epsilon^2} \propto T^{\lambda(1-m-1\gamma)}$$

and

$$t^{\lambda}\sqrt{\epsilon} \propto 1.$$

By combining these two relationships, we find that the long-time scaling of the minimum gap width is given by

$$\epsilon \propto T^{-2/(1+m+1/\gamma)}. \tag{99}$$

In the case of a fluid with constant *dynamic* viscosity, we requite that $m = -1/\gamma$, so we recover the $\epsilon \propto T^{-2}$ scaling obtained in the incompressible case, regardless of the value of γ. If instead we assume that the *kinematic* viscosity remains constant, then $m = 0$, and the exponent in (99) is strictly greater than -2 for all (positive) values of γ. In this latter case, the settling velocity is decreased due to the increase in dynamic viscosity that arises when the fluid is compressed. The similarity scaling (99) has been verified against a direct integration of the partial differential equation (95) in the case of both constant dynamic viscosity and constant kinematic viscosity.

In summary, compressibility does not appear to provide a means by which a contact can be made in finite time. Indeed, it is difficult to improve on the $\epsilon \sim T^{-2}$ approach obtained in the incompressible problem described in §1. Whilst compressing the fluid can alleviate some of the pressure beneath the settling object, there is an associated increase in dynamic viscosity that provides a greater resistance to flow. This, in turn, increases the pressure beneath the object, slowing its approach.

5 Conclusions and future work

At the outset, the intention of this project was to consider whether simple hydrodynamical effects could resolve the problem of infinite contact time for two solid objects coming together in a viscous fluid. We chose to avoid a discussion of short-ranged effects such as Van der Waals forces, in favour of the effects of the shape and elasticity of the objects, and compressibiliy of the fluid. Of these three effects, it seems that only shape, in the form of sharp aperities, can resolve this long-standing problem.

We have shown that an object with discontinuous first derivative will settle towards a flat surface in finite time by considering the model problem of a sedimenting triangular

wedge. However, we considered a constrained problem, in which the wedge was not allowed to change its orientation relative to the ground. Given that the wedge would be unstable to toppling in one direction or the other, it would be interesting to examine the motion of the wedge in the unconstrained problem, where the wedge is entirely free to move. Would contact still occur in finite time, or would the wedge orient itself so that one of its edges becomes parallel to the ground, thus leading to an infinite contact time? Many of the methods discussed in §2.1 could be used to model the falling wedge, including both the outer Stokes approximation and the numerical scheme presented therein. This remains as a strong candidate for future work.

During the GFD Prgoram, we expended some time and effort on modelling the rolling of a rough cylinder next to a horizontal surface. We found that the presence of roughness can, in certain cases, either result in contact in finite time or no contact at all. While a more thorough investigation of how asymmetric roughness must be in order to cause these effects would be an interesting avenue for future study, our key results were essentially pre-empted by Zhao *et al.* [6]. Once again, we direct the reader to this paper for a more developed version of the results of §2.2.

The effects of material elasticity and fluid compressibility were investigated briefly, but it was found that neither could provide a mechanism by which contact could be achieved in finite time. However, our analysis of the problem with elastic boundaries suggested that it is possible to avoid contact entirely, provided that there is a sufficiently large force acting perpendicular to the line of closest approach of the two objects. The physics behind this effect is well described by the work of Skotheim & Mahadevan [4].

In summary, it appears that only surface roughness can predict finite time contact without resorting to non-hydrodynamical effects. Even then asperities must be perfectly sharp in order to make contact. For real surfaces, of course, no such sharp corners exits on (and above) the molecular scale, so it is the opinion of the author that one will be drawn inevitably towards the consideration of long range forces, and the dewetting of the by then very thin film between the two objects. This problem remains as a challenge to future researchers.

I would like to take the opportunity to thank everyone involved with this year's GFD Program for a thoroughly enjoyable summer. In particular, I should like to thank Neil for his mathematical guidance and outstanding singing ability[2]; George, Charlie and Phil for their patience and encouragement on the softball field; and Maha, Joe, and Bill for useful discussions. Finally, I would like to thank my fellow Fellows for being a lovely group of people to get to know over the summer, as well as being useful sounding boards for my 'obvious' mathematical deductions.

References

[1] G. K. Batchelor, *An introduction to fluid mechanics*, Cambridge University Press, 1967.

[2] D. Gérard-Varet and M. Hillairet, *Regularity issues in the problem of fluid structure interaction*, ArXiv e-prints, 805 (2008).

[2] Video evidence of which may be available electronically from the author, unless Neil gets to him first.

[3] F. Plouraboué and M. Boehm, *Multi-scale roughness transfer in cold metal rolling*, Tribol. Int., 32 (1999), pp. 45–57.

[4] J. M. Skotheim and L. Mahadevan, *Soft lubrication: The elastohydrodynamics of nonconforming and conforming contacts*, Phys. Fluids, 17 (2005), p. 092101.

[5] H. A. Stone, *On lubrication flows in geometries with zero local curvature*, Chem. Engng. Sci., 80 (2005), pp. 4838–4845.

[6] Y. Zhao, K. P. Galvin, and R. H. Davis, *Motion of a sphere down a rough plane in a viscous fluid*, Int. J. Multiphase Flow, 28 (2002), pp. 1787–1800.